



HAL
open science

Numerical modelling of entangled carbon fibre material under compression

Fadhel Chatti, Dominique Poquillon, Christophe Bouvet, Guilhem Michon

► **To cite this version:**

Fadhel Chatti, Dominique Poquillon, Christophe Bouvet, Guilhem Michon. Numerical modelling of entangled carbon fibre material under compression. *Computational Materials Science*, 2018, 151, pp.14-24. 10.1016/j.commatsci.2018.04.045 . hal-01880449

HAL Id: hal-01880449

<https://hal.science/hal-01880449>

Submitted on 29 Jan 2019

HAL is a multi-disciplinary open access archive for the deposit and dissemination of scientific research documents, whether they are published or not. The documents may come from teaching and research institutions in France or abroad, or from public or private research centers.

L'archive ouverte pluridisciplinaire **HAL**, est destinée au dépôt et à la diffusion de documents scientifiques de niveau recherche, publiés ou non, émanant des établissements d'enseignement et de recherche français ou étrangers, des laboratoires publics ou privés.



Open Archive Toulouse Archive Ouverte (OATAO)

OATAO is an open access repository that collects the work of some Toulouse researchers and makes it freely available over the web where possible.

This is an author's version published in: <https://oatao.univ-toulouse.fr/21829>

Official URL: <https://doi.org/10.1016/j.commatsci.2018.04.045>

To cite this version :

Chatti, Fadhel and Poquillon, Dominique and Bouvet, Christophe and Michon, Guilhem Numerical modelling of entangled carbon fibre material under compression. (2018) Computational Materials Science, 151. 14-24. ISSN 0927-0256

Any correspondence concerning this service should be sent to the repository administrator:

tech-oatao@listes-diff.inp-toulouse.fr

Numerical modelling of entangled carbon fibre material under compression

Fadhel Chatti^a, Dominique Poquillon^b, Christophe Bouvet^{a,*}, Guilhem Michon^a

^a Institut Clément Ader, CNRS UMR 5312, Université de Toulouse, ISAE-SUPAERO, 3 Rue Caroline Aigle, 31400 Toulouse, France

^b CIRIMAT, Université de Toulouse, INP-ENSIACET, 4, allée Emile Monso, BP 44362, 31432 Toulouse Cedex 4, France

ABSTRACT

Keywords:

Entangled fibres
Core material
RVE
Finite element model
Compression

A new entangled cross-linked material was recently developed in order to present a new core material that can resolve the drawbacks of the honeycomb. The optimization of entangled carbon fibres requires a deep understanding of the influence of the parameters of a fibre network on its macroscopic behaviour. This paper presents a 3D finite element model to investigate the compressive behaviour of this fibrous material. The current work focuses on a representative volume element (RVE) with appropriate boundary conditions and initial fibre distribution close to that of the experimental test. The morphology of the RVE is examined before loading. The simulation results show a good correlation with the experimental data in terms of stress-strain curves. The descriptors of the morphology such as the distance between contacts and fibre orientation are studied under compression loading.

1. Introduction

Sandwich structures are of great interest due to their attractive benefits, which include high stiffness to weight ratios [1,2]. As a result of these advantages, the use of composites has improved greatly in structural applications, first of all in the aerospace field.

Honeycomb is widely used as a core material in sandwich structures due to its good cost benefit ratio and its high stiffness for bending solicitations. Although this cellular material presents attractive properties, its implementation in complex structures and its quality control process are often difficult. Other drawbacks of this material are the low vibration damping and the closed porosity, which can induce condensation in operating conditions.

Recently, Mezeix [3,4] developed a new material in which carbon fibres were first entangled (Fig. 1) and then cross linked (Fig. 2) with epoxy resin to increase the stiffness for compression solicitations. Although this material offers many advantages that provide solutions to the drawbacks of the honeycomb, such as open porosity, adaptability to complex structures, and good vibration damping [5], it cannot substitute for honeycomb in the aerospace field due to its low stiffness for compression solicitations. In order to understand and optimize the behaviour of this material, a numerical study seems necessary and this current work presents the first step in its modelling. Unlike honeycomb, which has been significantly studied [6,7], limited researches [8,9] have been conducted to study and understand fibrous materials because of their complex tangled geometry.

The manufacturing process that will be presented later in Section 2

does not allow blocking of all the fibre fibre contacts by the epoxy junctions (cf. Fig. 2). That is why we can find two types of interactions between fibres in the entangled cross linked material. The first is the interaction through the cross links and the second is the friction between fibre surfaces. Piollet [5] has concluded that this second type of interaction is responsible for the promising vibration damping of such material. Frequent fibre fibre contacts without cross links exist initially in the material and their number can grow significantly under loading. This growth is mainly due to the deformation of the fibres, which induces new fibre to fibre contact, but also, at larger strain, due to the breaking of some epoxy junctions. This allows some fibres to move more freely and then to touch others fibres. These fibre fibre interactions have a noticeable effect on the macroscopic behaviour. A numerical study of fibre networks without cross links can have considerable importance and can bring a first idea about the influence of fibre fibre contacts without junctions on the behaviour of the cross linked material.

This investigation is based on a representative volume element (RVE) because macroscopic stresses and strains can be determined by the microscopic stresses and strains over a representative cell unit. Hill [10] concluded that the complex computation can be reduced by the use of RVE as a full scale model.

The first model of the uniaxial compression of 3D randomly oriented fibre assembly was developed by van Wyk [11]. It is based on the bending of fibres between contacts but does not take into account the fibre friction, the slippage, or the fibre twisting. Van Wyk does not include the frictional forces between fibres and he considered the

* Corresponding author.

E-mail address: christophe.bouvet@isae.fr (C. Bouvet).

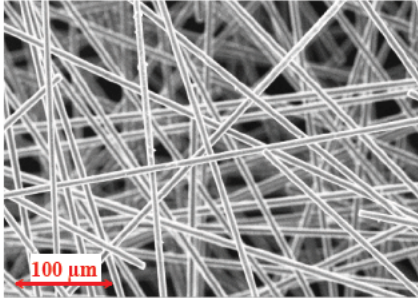


Fig. 1. Scanning electron microscope observation of entangled carbon fibres before packing operation.

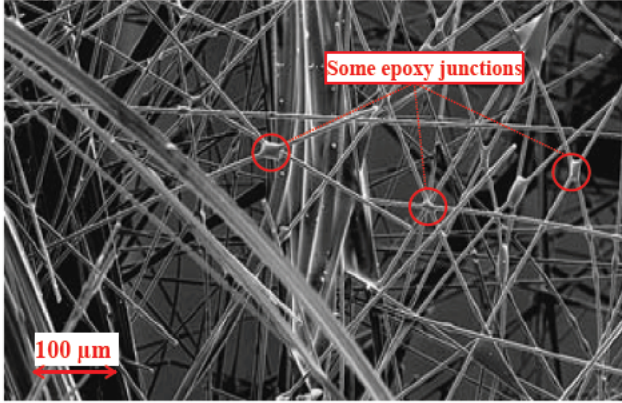


Fig. 2. Scanning electron microscope observation of entangled cross-linked carbon fibres.

distance between contacts to be proportional to the fibre volume fraction. He proposed the following equation, which presents the relationship between pressure and volume:

$$P = kE_{fibre}(f^3 - f_0^3) \quad (1)$$

where k an empirical constant, E_{fibre} is the fibre elastic modulus, f is the fibre volume fraction, and f_0 is the initial fibre volume fraction, that is to say the fibre volume fraction without any forces at the maximum unforced packing. Van Wyk concluded that his theory is valid only for a moderate fibre volume fraction lower than 10%.

Komori and Makishima [12] developed a theory that takes into account the fibre direction in different configurations in order to predict the number of fibre to fibre contacts in fibre assemblies. However, they do not predict the mechanical properties of the fibre network. The applicability of this theory is limited because it assumes affine deformation of the contact points between the fibres and it is only available for axial compression loading. Ning Pan [13] reported that the prediction of the number of contacts is too high in Komori and Makishima's theory. He proposed a modified approach to provide predictions of microstructural characteristics of fibre assemblies. He studied three different fibrous systems: ideal twist yarn, 2D random structure, and 3D random assembly, which can be a great basis for investigations of the properties of practical fibre assemblies. Lee, Carnaby, and Tandon [14] analysed the compression of a random fibre assembly using the bending energy while neglecting the crimp. Their model shows that if only fibre crimp is increased for a generated initial geometry, the tangent compression modulus actually decreases. A micro mechanical theory based on a statistical investigation of the distribution of contacts was developed by Toll [15]. He assumes that there is no statistical correlation between the height of particle and the distribution of the incremental forces. This assumption is a limitation of his approach because it can break down if the individual particles differ greatly in stiffness or size. Toll proposed an approach to calculate the

number of contacts per fibre for slender fibres:

$$N_c = \frac{8}{\pi} f r g \quad (2)$$

where f is the fibre volume fraction, g is a constant depending on the fibre orientation distribution, and r is the fibre aspect ratio. Beil and Roberts [22] carried out a numerical simulation of the uniaxial compression of a fibre assembly. In their model, the frictional and repulsion forces are used to model the fibre contact points. Their results show that the number of contacts in the assembly increases at a higher rate than that predicted by van Wyk. Their numerical model is limited to modelling a low volume fraction of $f = 0.8\%$ and its computational cost is very high. Barbier et al. [16,17] used discrete element simulations for a larger volume fraction of up to 35% but for assemblies of only 250 fibres with a small aspect ratio (20) because of the computational cost. Durville [18] proposed a finite element approach that discretizes the contact friction interactions from intermediate geometries to simulate the mechanical behaviour of beam assemblies. The application of this approach to the simulation of knot tightening proves that it is able to model the mechanical behaviour of fibrous materials. Recently, Abd El Rahman and Tucker [19] presented a numerical model of a fibre network which advanced the understanding of the evolution of microstructure under deformation. Although this model can be used for a high volume fraction of $f = 25\%$, it was not compared with experimental data. Their numerical results are affected by fibres coming out of the simulation box. This loss of fibres can have an impact on the stress, fibre distribution, and number of contacts.

2. Material and methods

2.1. Manufacturing process

In the present work, the entangled material is made with carbon fibres which provide high mechanical performance. The filament diameter is $7 \mu\text{m}$ and the elastic modulus is 240 GPa. A Mettler balance ($\pm 0.1 \text{ g}$) is used to weigh the samples. Microscopic observations of entangled material are carried out using an FEI Quanta 450 scanning electron microscope operating at 15 kV.

Mezeix [3] introduced the process of manufacturing. First of all, carbon yarns are cut to a fixed length of 12 mm. Many fibre lengths were tested before choosing the size of 12 mm which guarantees the best separation and entanglement of the fibres [3,4]. Then, carbon fibres are simultaneously separated from the received yarns and entangled in a 64 L blower room by manual application of compressed air. The air flow pressure is 6 bar. Fig. 1 shows a scanning electron microscopic observation of the separated entangled fibres. The contacts between fibres are not glued and so the fibres are free to move. We will focus just on the entangled material without cross links in this current work, which will be considered as a first investigation of the influence of microstructural properties in the global behaviour of the assembly. This first step is necessary before blocking (see Fig. 2) some points of contact with epoxy junctions as this gluing is done on an assembly of fibres that has been submitted to prepacking during a first compression step.

2.2. Experimental set up

The entangled fibres are placed in a cylindrical cell to be tested as shown in Fig. 3a. The two pistons are made of PVC (polyvinyl chloride), while the cylinder is made of PMMA (polymethyl methacrylate). The inner diameter of the cylinder is equal to 60 mm, which is five times larger than the fibre length. The entangled fibre sample can be compressed within the cell to different volume fractions by means of a movable piston. Initially, a mass of 9 g of entangled fibres is packed manually in the cylinder. The upper piston is moved down until a volume fraction equal to 6% is obtained. This process induces a

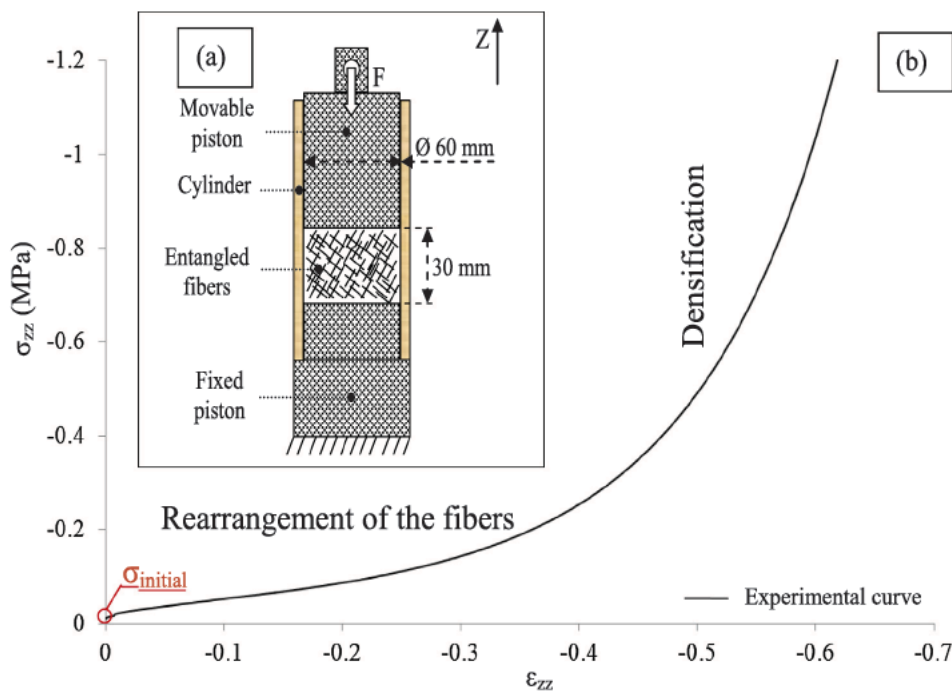


Fig. 3. (a) Cylindrical cell for compression test. (b) Example of experimental mechanical response of the entangled material fibre under compression, emphasizing the rearrangement step and then the densification of the assembly.

modification of the initial isotropic distribution of the fibre orientation. In the next section, this new distribution will be determined numerically with an original technique. Fig. 3b shows an experimental curve corresponding to a representative compression test carried out at 0.08 mm per second. Due to the initial packing, the initial stress σ_{initial} is different from zero. It is equal to -0.03 MPa. This value is measured at the end of fibre packing and exactly at the height of 30 mm of the fibre assembly. It corresponds to the stress required to obtain a volume fraction of 6%. Under increasing compression, the fibres begin to be rearranged until a deformation value of about -0.4 is reached. After that, a phase of densification occurs in which the stress increases more significantly with strain.

3. Direct numerical simulation method

A whole sample of entangled material of the size indicated in Fig. 3a contains 11 million carbon fibres and a great number of contacts. In this case, the numerical modelling of an entire sample would incur a high computational cost and would be complicated. Therefore, we have chosen to model a representative volume element (RVE), taking into account the appropriate boundary conditions and the representative initial fibre orientation distribution in order to be closer to the real conditions of experimental tests. A morphological study of the assembly of entangled fibres is carried out to choose the appropriate size of this RVE, which is then compressed. So we have to cope with a model taking into account large deformation and geometric nonlinearity.

The nonlinear finite element solver in ABAQUS/Explicit is used for simulation for two reasons. Firstly, it offers us the possibility of using large deformation beam elements. Secondly, it is efficient to capture and model the several contacts via its general contact algorithm. Each fibre is modelled by a variable number of 3D Timoshenko beam elements (B31 [21]) depending on both the number of contacts and on its orientation (see Fig. 4) in the RVE that determines its length in the computation.

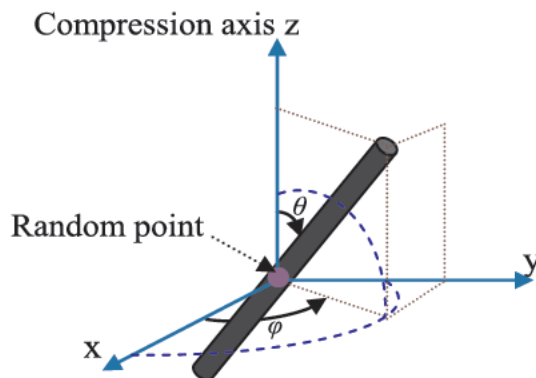


Fig. 4. Definition of polar and azimuthal angles of fibre.

3.1. Generation of initial geometry

The geometry of the RVE is generated with an in house pre processing program written in FORTRAN language. It is in cubic form with an edge length of l (cf. Fig. 5). Different values of l are tested to choose the most appropriate size for the RVE and at the same time minimize the calculation cost. The whole investigation is carried out and detailed in the next section, and finally the length $l = 1$ mm is adopted. The generation of the fibre assembly by in house preprocessing is as follows. First, a random point, which is presented in purple¹ colour in Figs. 4 and 5, is picked in the cube. Then, two angles θ and φ are chosen to create an isotropic fibre distribution. θ is the angle between the fibre direction and the compression axis z , while φ defines the angular direction of the fibre relative to the axis x .

The isotropic fibre distribution is generally presented by sine form [20]. It is characterized by more fibres that have an angle of $\theta = \frac{\pi}{2}$ in relation to the compression axis z . In Fig. 6, the comparison between the orientation of the numerically generated fibres and the theoretical

¹ For interpretation of color in Figs. 4, 5 and 10, the reader is referred to the web version of this article.

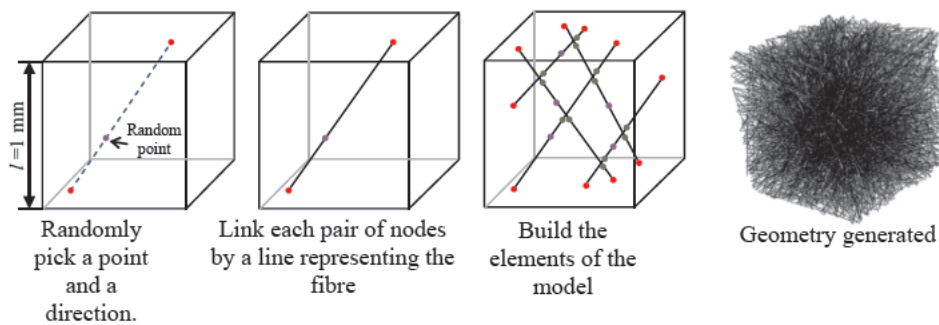


Fig. 5. Principle of generation of the fibre network.

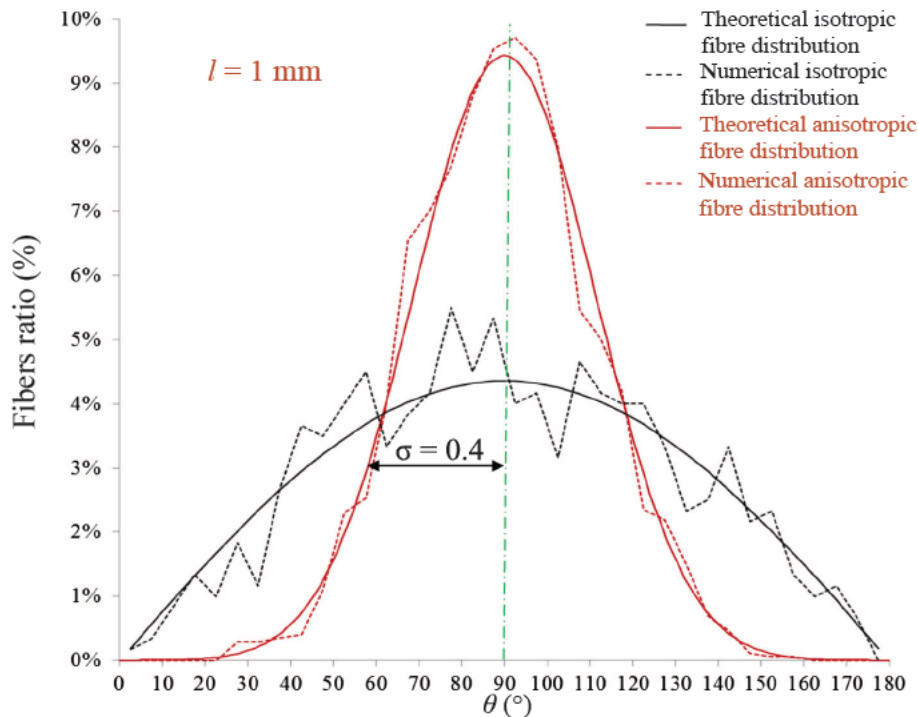


Fig. 6. Comparison between the numerical results and the theory for isotropic and anisotropic fibre distribution.

isotropic orientation shows a good correlation. This point has been verified on several different draws. As the volume is cubic and not spherical, it was important to verify that this choice did not induce any bias. The numerical curve becomes closer to the theoretical one when the size of the RVE is larger. The final choice of the length l is based on the best isotropic morphology with the lowest calculation time. It is a compromise between the accuracy of the description of the morphology of the material and the calculation cost. This choice of the size of RVE will be specified in the next part and will be used thereafter in all numerical simulations of compression.

Straight fibres are generated in the cube. Each fibre is delimited by two intersection points between its directions and the faces of the box. These points are presented in red colour in Fig. 5. When the distance between two fibres is less than the diameter of the fibre then two nodes, coloured green in Fig. 5, are created on each fibre. These points allow the fibre to be cut into segments of different lengths. Each segment corresponds to a beam element of the model. Some nodes can be cancelled if the elements limited by them are very small. The length of these elements should be twice as long as the fibre diameter in order to avoid the use of very low time steps in explicit calculation. So this condition makes it possible to minimize the computational cost. Fig. 5 presents the different steps of fibre network generation in a box of $1 \times 1 \times 1 \text{ mm}^3$ size.

For the anisotropically distributed fibres, the method of fibre generation is the same as in the isotropic case except that the fibre direction θ follows a different law. The sine form is replaced by a Gaussian distribution, as shown in Fig. 6. This modelling has been chosen after the first compression simulations. In the Gaussian distribution, there are more fibres around the angle $\theta = 90^\circ$ than in the isotropic case because many fibres lose their vertical orientations during the packing/compression process. As a matter of fact, the peculiar shape obtained for the distribution of the fibre orientations after increasing compression seems well represented by a Gaussian function. So, for the generation of an anisotropic assembly of entangled fibres, the angles θ are calculated from the following Gaussian distribution:

$$g(\theta) = \frac{\sin\theta}{2} \times e^{-\frac{(\theta - \frac{\pi}{2})^2}{2\sigma^2}} \times A \quad (3)$$

where A is a constant such that $\int_0^{180} g(\theta)d\theta = 1$ and the standard deviation σ depends on the compression ratio. For the experimental data of this study, the value of σ equals 0.4. This value is determined from the numerical investigation carried out in the next section.

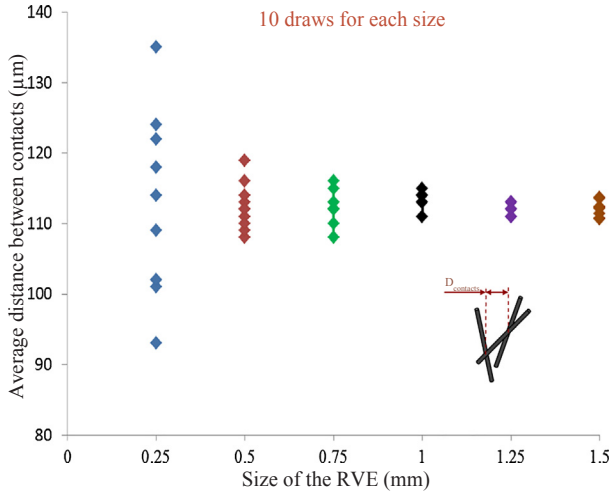


Fig. 7. Investigation of the average distance between contacts for a material with a volume fraction of 6%. For each RVE size, 10 different morphologies are generated.

3.2. Determination of the size of the morphological RVE

3.2.1. Distance between contacts

The RVE is widely used to predict the properties of random material. It is important to determine the proper size of RVE which will provide a structure with stable morphological characteristics. One of the most important characteristics is the average distance between contacts, which influences the macroscopic behaviour of the material. Mezeix [3] has shown by his microscopic observations that the observed average distance between contacts for entangled carbon fibres with a volume fraction of 8.5% is 120_{-70}^{+140} µm. The tolerance interval of this value confirms the large dispersion he observed. In our morphological study, we have chosen different sizes of RVE in ascending order. For each case, 10 different draws are generated, so 10 different fibre entanglements with a fibre volume fraction of 6% are studied. The average distance between contacts is calculated for each draw. The numerical results, as illustrated in Fig. 7, show that this parameter converges to the value of 112 µm. This value is not far from the one found by Mezeix in his investigation. For RVEs larger than 1 mm, the dispersion between draws is less than 5%. When the size is smaller, the values of the average distance between contacts become dispersed. A cubic box with sides of 1 mm seems to correctly represent the morphology of the assembly and is kept as the RVE for the rest of the study. It is the smallest size that can offer a stable value of distance between contacts for each draw with the minimum number of elements. This choice allows the calculation cost to be minimized.

3.2.2. Distribution of fibre orientations

Another key parameter that needs to be studied is the distribution of fibre directions. As 10 draws have been generated for the cubic RVE with a size of 1 mm and fibre volume fraction of 6%, for each of them, corresponding to different colours in Fig. 8, the proportion of fibres in each interval of θ , the angle between the fibre direction and the compression axis z , is plotted. The angular amplitude is divided into 36 regular segments of 5° . The black curve is the theoretical curve of a random fibre assembly. A good correlation is obtained between the theory and the FORTRAN in house preprocessing program used to generate the random geometry in terms of the distribution of the fibre directions.

In order to quantify the difference between the generation of numerical fibres and the theoretical sine distribution, a deviation measure is defined as:

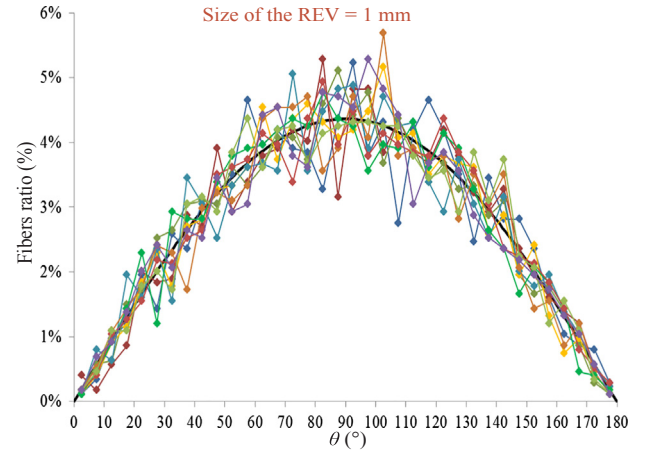


Fig. 8. Distribution of the fibre directions of the 10 random geometries generated for an RVE with sides of 1 mm.

$$Deviation = \sum_i \frac{(Fibersratio(\theta_i) - \sin(\theta_i))^2}{\sin(\theta_i)} \quad (4)$$

The fibre orientation is studied for all the fibre assemblies generated for the different RVEs. The deviation versus size is plotted in Fig. 9 for the 10 draws of each RVE. The deviation converges to zero and once again an RVE size of 1 mm³ appears to be a good compromise to describe the morphology with accuracy while reducing the computational time.

3.3. Determination of the initial distribution of fibre orientations

At the end of fabrication in the compression device, the entangled and packed carbon fibres no longer have an isotropic distribution of fibre orientations. The initial isotropic distribution is indeed modified when the fibres are placed in the cylindrical cell (cf. Fig. 10) and compressed to a height of 30 mm to get the target initial volume fraction of 6%. Before the fibre packing process, the height of the entangled sample placed in the cylindrical cell is about five times higher than the height necessary to obtain a volume fraction of 6%. A preliminary numerical study is then carried out to identify the new distribution of the fibre orientations after the packing process. Then, a RVE in parallelepiped shape is generated with an isotropic fibre distribution, which is presented in Fig. 10 by the bold dashed black curve. Its height is five times greater than the usual height and its section dimensions are

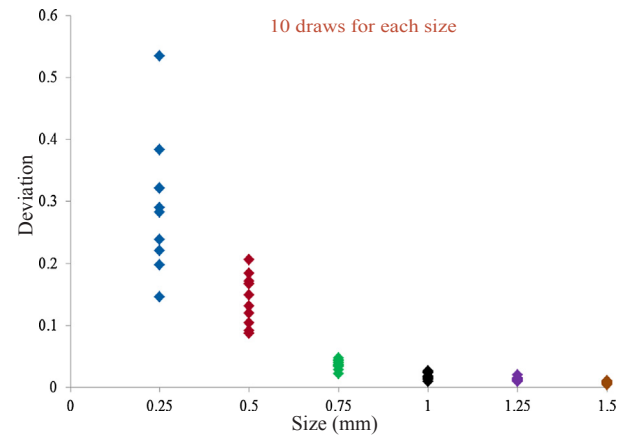


Fig. 9. The influence of the RVE size on the deviation of fibre orientation of the numerically generated geometries compared to the theoretical sine distribution corresponding to the isotropic distribution of fibres. See Eq. (4) for the definition of the deviation.

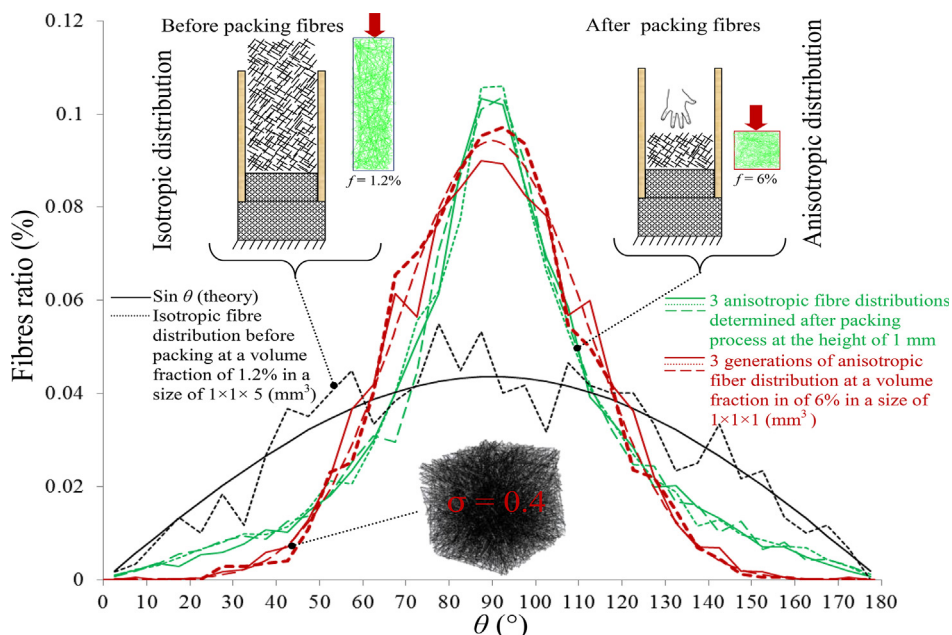


Fig. 10. Numerical determination of the fibre orientation distribution.

Table 1

Mechanical properties of carbon fibre.

Density, ρ	1770 kg/m ³
Elastic modulus, E	240 GPa
Poisson's ratio, ν	0.3
Friction, μ	0.05

$1 \times 1 \text{ mm}^2$. So its volume fraction is five times smaller than the one adopted at the beginning of experimental loading and equals 1.2%. After the isotropic generation of fibres in this RVE, it is compressed axially until a height of 1 mm is obtained, which provides a volume fraction of 6% and the distribution of the fibre directions that will be used initially for the simulation with the $1 \times 1 \times 1 \text{ mm}^3$ RVE. The numerical modelling is carried out in ABAQUS/Explicit, which is a good tool for managing the geometric nonlinearity accompanied by the contact phenomenon. The compression is carried out from 5 to 1 mm with high velocity in order to minimize the calculation time. We have to stop the simulation at this level and do not continue the compression because it is difficult to achieve convergence of the calculation when the height of 1 mm is reached. The use of 3D explicit finite element analysis requires a dynamic investigation and a fixed time step which is linked to the smallest element. At the height of 1 mm, the time step fixed in the beginning of the simulation seems to be not less than the time needed for the wave to go across the smallest element and so the Courant Friedrichs Lewy (CFL) stability condition cannot be satisfied [21]. Therefore, a new geometry with a size of $1 \times 1 \times 1 \text{ mm}^3$ is created. The fibres in this new geometry (see green curves of Fig. 10) are generated in such a way that the distribution is Gaussian and representative of the one obtained after the initial packing process (see the red curves in Fig. 10). The comparison between the anisotropic fibre distribution used and the one found after the packing process shows a slight difference. We do not generate the exact anisotropic distribution found after the packing of the fibres; it would have used a function much more complex than the Gaussian function (3). But the result that is found with a standard deviation $\sigma = 0.4$ remains a good approximation to the desired anisotropic fibre distribution.

3.4. Explicit simulation

All simulations are performed in ABAQUS/Explicit, which is

efficient for the problem of large deformation with several mechanical contacts. Each simulation uses 20 parallel processors and 3 GB of memory per processor and lasts about 16 h. The RVE size is $1 \times 1 \times 1 \text{ mm}^3$ and 1710 carbon straight fibres are generated inside in order to have a targeted initial volume fraction of 6%. The fibre lengths are variable (its mean is 0.9 mm) and the fibre diameter is equal to $7 \mu\text{m}$. Indeed, if the real fibre length is 12 mm, in the simulation the fibres pass through the box and thus have lengths which vary with their initial orientation. The fibre mechanical properties used in the simulation are shown in Table 1.

The geometry is surrounded by six rigid faces to be close to the boundary conditions of the experimental. In Fig. 11, these faces are

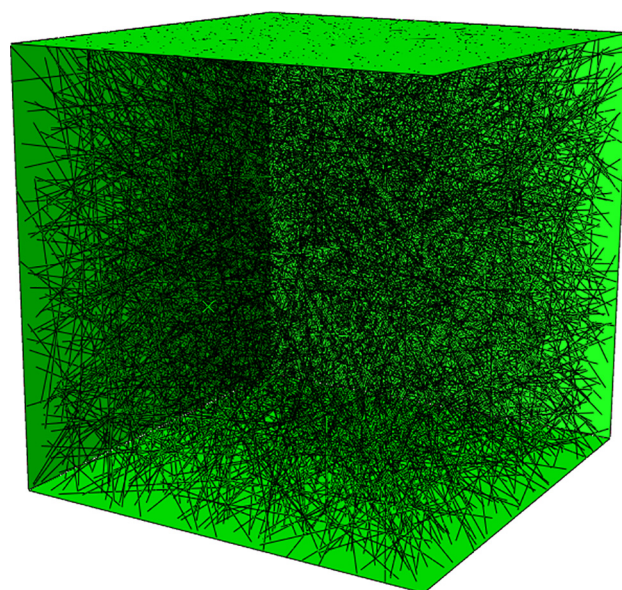


Fig. 11. Rigid surfaces in green that surround the geometry containing 21,549 beam elements and prevent the fibres leaving the box during the compression process. The z axis is vertical and is the direction of compression. The upper surface moves downward to compress the fibres. (For interpretation of the references to colour in this figure legend, the reader is referred to the web version of this article.)

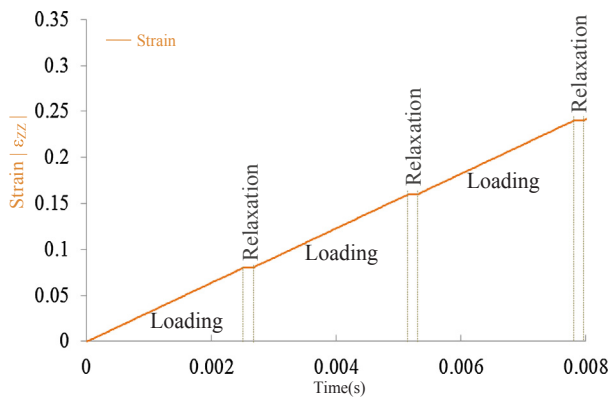


Fig. 12. Loading process of the finite element model.

presented in green colour and two faces are removed to show the geometry of the assembly of fibres generated inside the box. Only the upper face can move along the compression axis z to impose the compression of the RVE.

The ABAQUS/Explicit [21] general contact algorithm is used to manage the interaction between pairs of fibres and the interaction of one fibre with itself. In order to have a no penetration condition, the “hard contact” type is chosen. The friction coefficient introduced is $\mu = 0.05$, which is often used for composite studies [22].

The choice of the loading time step is very important in the use of ABAQUS/Explicit. It is a principal key to have a quasi static response with the lowest computational cost. ABAQUS/Explicit is usually considered as a good tool in dynamic analysis but it can be relevant in quasi static studies if appropriate conditions are respected. The kinetic energy of the whole finite element model is followed during the deformation in order to verify that it remains low compared to the other energies. A special technique of loading is adopted, as shown in Fig. 12. The applied velocity is imposed in successive steps. Between each two consecutive loading steps, a relaxation plateau is introduced in order to stabilize the structure and to reduce the kinetic energy (Fig. 13). During this plateau, successive steps of relaxation are imposed. Between each two consecutive relaxation times, the motions of all nodes are stopped in order to avoid the divergence of the kinetic energy. This method allows the convergence of the kinetic energy to zero at the end of each plateau and ensures that the system inertia does not affect the compressive stress.

Fig. 13 illustrates the imposed strain, the kinetic energy, and the compressive stress of a confined compression test. In this simulation, the size of the RVE is $1 \times 1 \times 1 \text{ mm}^3$ and the initial fibre distribution is anisotropic, as shown in Fig. 10. Only the three first loading steps are retained in Fig. 13 to show clearly the convergence of the curves during the relaxation steps.

The total physical time used in the loading step is equal to 0.0025 s and the time increment chosen to have a strain rate much less than the wave speed is $0.01 \mu\text{s}$.

In the simulations, the material density is increased artificially in order to control the time increment. The use of mass scaling makes it possible to achieve an economical solution for the expensive computational cost [21]. The simulation requires 250,000 time increments for a loading step with 8% strain and 2000 time increments for each relaxation step in the plateau. The total duration of the simulation is about 16 h.

4. Results and discussion

4.1. Compression test

The initial packing process has induced anisotropy, which is emphasized during the following compression. As illustrated in Fig. 14, the

fibre rearrangement is noticeable and more and more fibres have a θ angle orientation that is close to perpendicular to the compression axis. The number of contact points increases and so the average distance between contacts decreases. The evolution of this parameter depends on the volume fraction and on the orientation distribution of fibres too. In these simulations, the friction coefficient is 0.05 and sliding at contact points is permitted. The friction coefficient of the fibre with the box surface is 0.05.

The stress versus strain curves (Fig. 15) give valuable information for the interpretation of the compression behaviour. The comparison between the numerical curve and experimental data presents a good correlation with respect to two phases: the first is the rearrangement of the fibres and the second is the densification. Numerically, the curve of stress versus strain is steeper than the experimental curve and the densification takes place earlier. This can be explained by two factors: first, the tortuosity of fibres, which is small but is not taken into account in the model, and second, the idealized morphology of the computations. In the real packing, not all of the fibres are perfectly separated and some very small yarns remain. The real material is then probably more heterogeneous than the numerical one. If areas with remaining yarns are denser, then some areas with fewer fibres are weaker and probably responsible for larger deformation. The initial stress is different from zero for the experimental curve due to the load applied in order to get an initial volume fraction of 6%. However, the rearrangement phase, which corresponds to the reorientation of the fibres, is properly modelled by the proposed simulation even if the initial stress found numerically is equal to zero because the load obtained at the end of the packing process has not been taken into account in the numerical modelling of the compression test.

The initial stiffness measured from the simulation curve is equal to 0.4 MPa. The numerical and experimental curves have almost the same slope. In Fig. 11, the two experimental curves are represented in black. One is plotted with a dashed line and the other with a solid line. These two curves confirm the repeatability of the experimental compression.

In order to study the macroscopic isotropy, three RVEs are solicited in compression; Table 2 presents the parameters of the three draws. The three curves of the stress versus strain have a similar shape to the experimental one with the two phases mentioned above (Fig. 16). There is a small dispersion between the three numerical results, which can be explained by the dispersion between the three initial geometries generated.

4.2. Evolution of the orientation of fibres during axial compression

Each fibre in the RVE is discretized in beam elements. Its orientation is determined by the accumulated segmental orientation. Fig. 17 shows the orientation of the segments of a fibre. A FORTRAN post processing program is developed to measure the segmental orientations. This program uses the nodal coordinates exported from ABAQUS/Explicit after the relaxation step. It calculates the angle θ between the direction of each segment of a fibre and the compression axis which corresponds to the direction $\theta = 0$. Then, it classifies the fibre direction θ (see Fig. 3) in intervals of 5° from 0° to 180° as has been done for the initial straight fibre orientation. The results obtained are plotted to present the ratio of fibre segments in each interval.

The orientation distribution functions at volume fractions of 6, 7.1, 8.8, and 11.5% are plotted in Fig. 18. The sine fibre distribution of an isotropic RVE is also plotted for comparison.

The distribution is Gaussian like in the range tested. As the fibre network becomes compressed, the volume fraction increases and the fibres are reoriented. We obtain more and more fibres whose direction is close to horizontal ($\theta = 90^\circ$) and thus perpendicular to the compression axis.

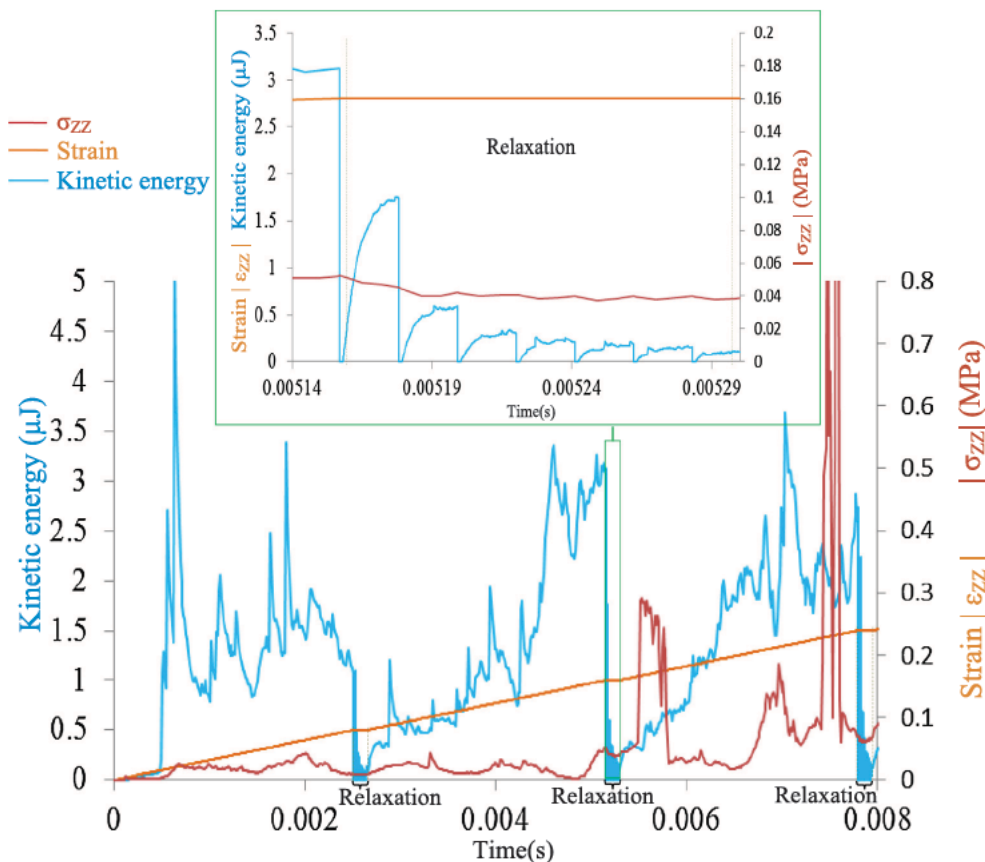


Fig. 13. Kinetic energy (blue), strain (orange), and stress (red) as a function of time. (For interpretation of the references to colour in this figure legend, the reader is referred to the web version of this article.)

4.3. Distance between contacts

ABAQUS/Explicit is unable to give the number of contacts in each time step directly. To define the contact statistics, a post processing program is used to evaluate the number of contacts. At the end of each relaxation step, the new coordinates of nodes' locations are searched. Then, the intersections between all elements are checked and the average distance between contacts is calculated by dividing the total length of fibres by the number of contacts.

In Fig. 19, the distance between contacts is compared to Philipse's theory [23].

$$D_{contact} = \frac{d}{f} \tag{5}$$

where f is the volume fraction and d is the fibre diameter.

Before the fibre packing and for a volume fraction of 1.2%, the average distance between contacts is close to the calculated value from Philipse's theory. This good agreement is explained by the orientation distribution of fibres, which is isotropic, as in Philipse's theory. During compression, there are more and more contacts between fibres, so the

distance between contacts decreases. The number of contacts is larger than that determined from the theory and so the results for the average distance between contacts during loading overestimate the theoretical results. This is logical because the Philipse's equation is used just for the isotropic case while the fibre orientation distribution is Gaussian with a smaller and smaller standard deviation during compression. After the packing of the fibres, the RVE reaches a volume fraction of 6% and the Gaussian distribution corresponds to $\sigma = 0.4$. At this level, the average distance between contacts is equal to 125 μm . The value of this parameter is equal to 115 μm when it is calculated theoretically for an isotropic case.

5. Conclusion

The purpose of the current work is to carry out the first step in the modelling of entangled cross linked fibres. The proposed model focuses on the influence of fibres which are in contact without an epoxy link on the behaviour of the entangled cross linked material. The investigations carried out here without cross linking are a robust base for understanding the behaviour of the entangled cross linked fibres later in

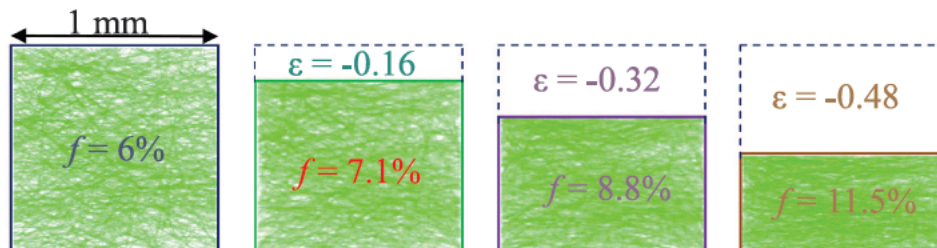


Fig. 14. Evolution of the RVE during compression.

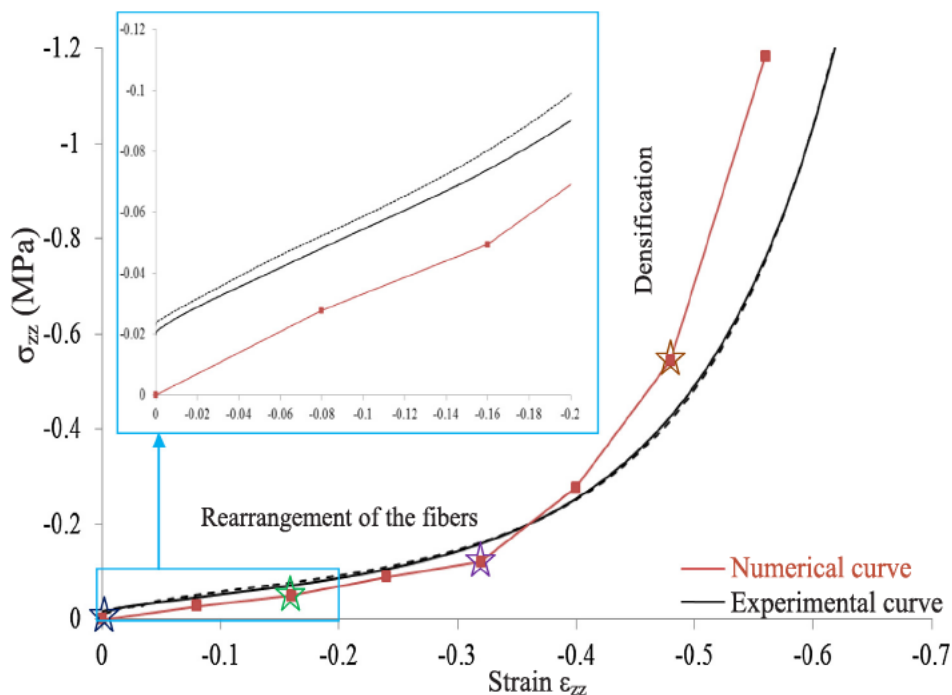


Fig. 15. Comparison of the stress-strain response between experimental results (solid and dashed black lines) and numerical data (red curve). (For interpretation of the references to colour in this figure legend, the reader is referred to the web version of this article.)

Table 2
Details of the three different simulations carried out.

RVE	Number of beam elements	Number of nodes	Average distance between contacts (μm)
RVE 1	21,549	23,231	122
RVE 2	21,417	23,126	123
RVE 3	20,986	22,688	125

order to enhance their mechanical properties.

A numerical model has been developed to predict the behaviour of entangled material in compression. It is a finite element model which uses 3D beam elements able to simulate all modes of fibre deformation

to take into account friction between fibres and to be applied to a large number of fibres.

The numerical model is developed in ABAQUS/Explicit, which is efficient for the nonlinear deformation and the management of several contacts. During numerical compression, each loading step is followed by a relaxation time, which is carefully chosen to obtain a quasi static response and to lead the system to equilibrium. This type of loading is necessary in explicit calculation of network fibres. A morphological study has been carried out to determine the size of the RVE.

In this study, the orientation distribution of fibres is generated initially to respect the experimental conditions as far as possible. A special numerical technique has been developed to find the appropriate Gaussian distribution for the initial geometry. It takes into account the positioning of fibres in the experimental apparatus, which causes the

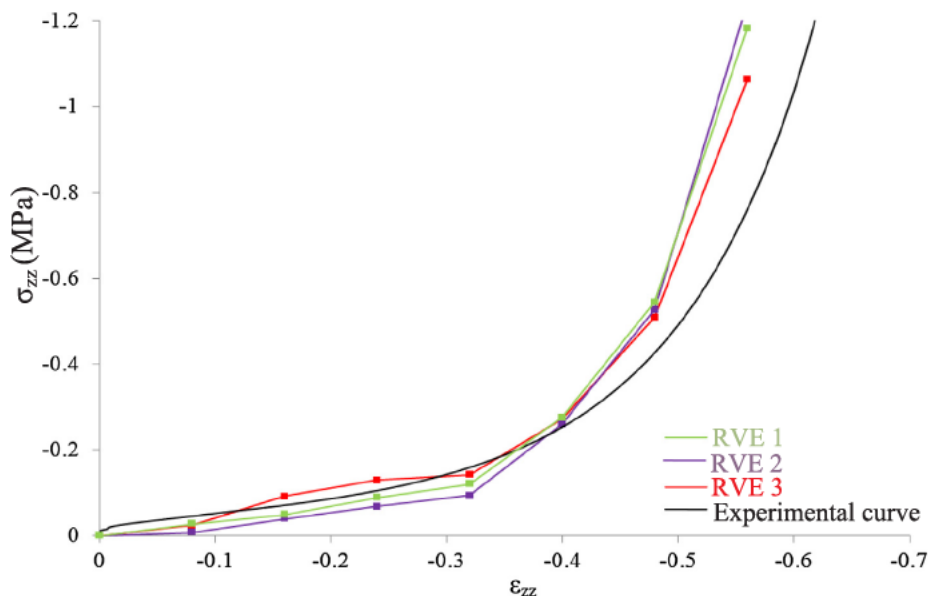


Fig. 16. Plots of stress versus strain for three different RVEs – comparison with an experimental curve.

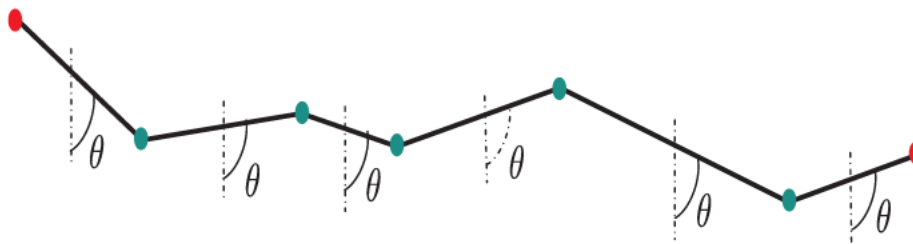


Fig. 17. Segmental orientation of a fibre: the orientation θ of each element of the fibre is calculated. The compression axis z is vertical.

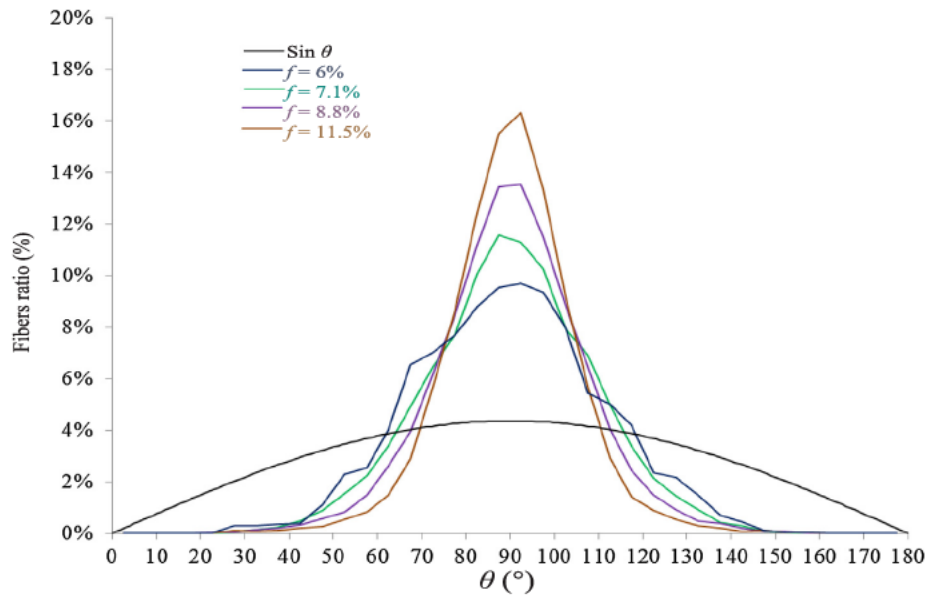


Fig. 18. Evolution of the orientation distribution of fibre segments during compression.

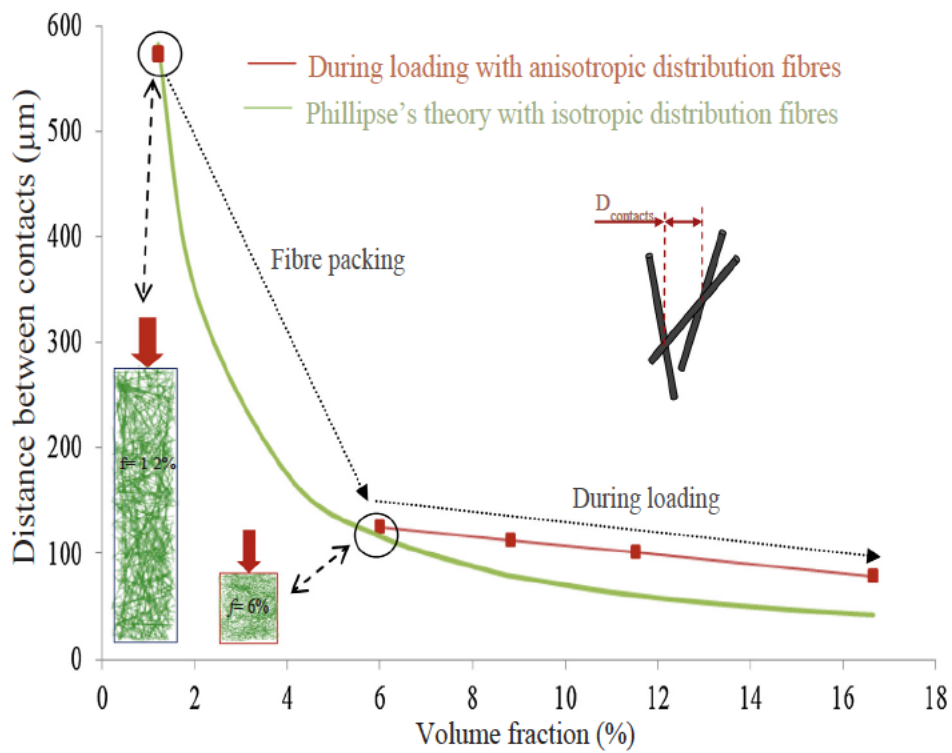


Fig. 19. Evolution of the average distance between contacts as a function of volume fraction: comparison of the data of this study and theoretical values.

loss of the morphological isotropy. A 3D tomography investigation is envisaged to confirm the numerical obtained results.

The numerical predictions of a compressed fibre network are compared with the results of experimental tests and a good agreement can be found between the two results. The numerical simulations provide a correct stress strain curve shape compared to that found experimentally. The orientation distribution of fibres and the distance between contacts are studied during the compression. This micromechanical study will allow for a better understanding of the influence of these parameters on the global behaviour of the entangled material and will make it possible to predict its impact on the macro mechanical properties of the entangled cross linked material and finally how we should manage these parameters to improve the manufacturing process to offer a better global behaviour. This improvement will make the entangled cross linked material relevant for use in structural applications as a core material.

Acknowledgements

Thanks are due to CALMIP for the support and the computing power. Financial support for this work was obtained thanks to the joint project MAFIVA funded by the Midi Pyrénées region and by ISAE Supaéro.

Data availability

The raw/processed data required to reproduce these findings cannot be shared at this time as the data also forms part of an ongoing study, but feel free to contact the corresponding author at christophe.bouvet@isae.fr to get them.

Appendix A. Supplementary material

Supplementary data associated with this article can be found, in the online version, at <http://dx.doi.org/10.1016/j.commat.2018.04.045>.

References

- [1] B. Castanié, Y. Aminanda, C. Bouvet, J.J. Barrau, Core crush criterion to determine the strength of sandwich composite structures subjected to compression after impact, *Compos. Struct.* 86 (1–3) (2008) 243–250.

- [2] S. Belouettar, A. Abbadi, Z. Azari, R. Belouettar, P. Freres, Experimental investigation of static and fatigue behaviour of composites honeycomb materials using four point bending tests, *Compos. Struct.* 87 (2009) 265–273.
- [3] L. Mezeix, C. Bouvet, J. Huez, D. Poquillon, Mechanical behavior of entangled fibres and entangled cross-linked fibres during compression, *J. Mater. Sci.* 44 (14) (2009) 3652–3661.
- [4] L. Mezeix, D. Poquillon, C. Bouvet, Entangled cross-linked fibres for an application as core material for sandwich structures part I: Experimental investigation, *Appl. Compos. Mater.* 23 (1) (2016) 71–86.
- [5] E. Piollet, D. Poquillon, G. Michon, Dynamic hysteresis modelling of entangled cross-linked fibres in shear, *J. Sound Vib.* 383 (2016) 248–264.
- [6] M.J. Silva, L.J. Gibson, The effects of non-periodic microstructure and defects on the compressive strength of two-dimensional cellular solids, *Int. J. Mech. Sci.* 39 (1997) 549–563.
- [7] L.J. Gibson, M.F. Ashby, *Cellular Solids: Structure and Properties*, Cambridge University Press, 1997.
- [8] S. Heyden, Network modelling for the evaluation of mechanical properties of cellulose fibre fluff, Ph.D. thesis Lund University, Sweden, 2000.
- [9] Y.H. Ma, H.X. Zhu, B. Su, G.K. Hu, R. Perks, The elasto-plastic behavior of three-dimensional stochastic fibre networks with cross-linkers, *J. Mech. Phys. Solids* 110 (2018) 155–172.
- [10] R. Hill, Elastic properties of reinforced solids: some theoretical principles, *J. Mech. Phys. Solids* 11 (1963) 357–372.
- [11] C.M. van Wyk, Note on the compressibility of wool, *Text. Res. J. Inst.* 37 (1946) T285–T292.
- [12] T. Komori, K. Makishima, Number of fiber-to-fiber contacts in general fiber assemblies, *Text. Res. J.* 47 (13) (1977) 13–17.
- [13] N. Pan, A modified analysis of the microstructural characteristics of general fiber assemblies, *Text. Res. J.* 63 (1993) 6.
- [14] D.H. Lee, G.A. Camaby, S.K. Tandon, Compressional energy of the random fiber assembly. Part II: Evaluation, *Text. Res. J.* 62 (1992) 258–265.
- [15] S. Toll, Packing mechanics of fiber reinforcements, *Polym. Eng. Sci.* 38 (8) (1998) 1337–1350.
- [16] C. Barbier, R. Dendievel, D. Rodney, Role of friction in the mechanics of nonbonded fibrous materials, *Phys. Rev. E* (July) (2009) 016115.
- [17] C. Barbier, R. Dendievel, D. Rodney, Numerical study of 3-D compressions of entangled materials, *Comput. Mater. Sci.* 45 (3) (2009) 593–596.
- [18] D. Durville, Contact-friction modeling within elastic beam assemblies: an application to knot tightening, *Comput. Mech.* 49 (2012) 687–707.
- [19] A.I. Abd El-Rahman, C.L. Tucker III, Mechanics of random discontinuous long-fiber thermoplastics. Part II: Direct simulation of uniaxial compression, *J. Rheol.* 57 (2013) 1463.
- [20] T.W. Clyne, I.O. Golosnoy, J.C. Tan, A.E. Markaki, Porous materials for thermal management under extreme conditions, *Philos. Trans. Roy. Soc. A* 364 (2006) 125–146.
- [21] *User Documentation, ABAQUS User's Manual: Version 6.11.*
- [22] M. Tournonias, M.A. Bueno, D. Poquillon, Friction of carbon tows and fine single fibers, *Compos. A Appl. Sci. Manuf.* 98 (2017) 116–123.
- [23] A. Philipse, The random contact equation and its implications for (colloidal) rods in packings, suspensions, and anisotropic powders, *Langmuir* 12 (1996) 1127–1133.